Chapter 6

Structure and thickness of the lithospheric mantle

6.1 Nature of the lithosphere and lithosphere-asthenosphere transition

The terms lithosphere and asthenosphere were originally defined with regards to rheology, with the lithosphere behaving essentially as an elastic solid, and the asthenosphere deforming as a viscous fluid (*Barrell*, 1914). Since then, additional, differing usages of the term lithosphere have been introduced such as thermal, seismic or chemical lithosphere (*Anderson*, 1995). In the context of plate tectonics, the lithosphere is defined as the crust and a part of the upper mantle that translate coherently on the Earth's surface (*Isaacs et al.*, 1968). The lithosphere behaves rigidly on geologic time scales of millions of years. The widely adopted thermal definition considers the lithosphere as a conductive layer above a convecting mantle and associates the lithosphere-asthenosphere boundary with an isotherm of about 1280°C (*McKenzie and Bickle*, 1988). The asthenosphere probably contains a small percentage of molten mantle material (peridotite). The lithosphere is seismologically defined as the high-velocity outer layer of the Earth. It comprises the Earth's crust and the uppermost high-velocity part of the Earth's mantle. At many places it is underlain by a region of diminished velocity or negative velocity gradient in the upper mantle (*Gutenberg*, 1926, 1959), the asthenosphere. While the seismic definition describes the lithosphere-asthenosphere boundary from the point of view of mean isotropic velocities, *Plomerová et al.* (2002) and *Gung et al.* (2003) explain the transition at the bottom of the lithosphere beneath continents as a change in anisotropic structure between frozen-in structure in the lithosphere and anisotropic structure from ongoing dynamic processes in the underlying asthenosphere. The lithosphere-asthenosphere boundary is furthermore associated with a layer of increased electrical conductivity due to partial melting (*Jones*, 1982; *Hjelt*, 1991; *Jones*, 1999, *ERCEUGT-Group*, 1992, *Simpson*, 2002).

As several physical parameters change at the bottom boundary of the lithosphere, it appears to be a significant discontinuity in the seismic stratification of the upper mantle (*Gaherty et al.*, 1999). Although various physical parameters need not necessarily describe the same boundary, several studies demonstrate an agreement between the lithospheric thickness as derived from seismological, thermal and electromagnetic observations (e.g. *Praus et al.*, 1990, *Babuška and Plomerová,* 1993).

So far, most information about the thickness of the lithosphere comes from low-resolution surface-wave observations. High-resolution seismic body-wave observations of

the lithosphere-asthenosphere boundary are very rare. This is in contrast to the Moho, which is globally a much better documented discontinuity. The thickness of the lithosphere is considered to be close to zero at mid-ocean ridges, up to about 200 km beneath stable cratons with 80 to 110 km being the global average. The asthenosphere probably extends in average to 150-250 km depths, where *S* wave velocity rises again to a value corresponding to rigid peridotite. *Lehmann* (1961, 1964) proposed the existence of a general discontinuity in the upper mantle, the Lehmann Discontinuity, at a depth of ca. 220 km. The base of the asthenospheric low velocity zone may correspond to the Lehmann discontinuity, which is shallow in cold, stable cratonic areas and deep in hot, active regions of the world according to *Thybo* (2006). The low velocity zone of the asthenosphere is much better developed under ocean basins than under continental shield areas where it is sometimes barely developed. Hence, oceanic lithosphere is much better defined seismologically than continental lithosphere.

However, velocity-depth profiles through the Earth's upper mantle do not define the top and bottom of the zones of rigid and viscous behaviour precisely because the zones have transitional boundaries. If the lithosphere is simply a thermal boundary layer that is more rigid owing to colder temperatures, mantle flow models (*King and Ritsema*, 2000; *Zaranek et al.*, 2004) indicate that the velocity gradient at its base would occur over tens of kilometres. In contrast, if the asthenosphere is weak owing to volatile enrichment (*Hirth and Kohlstedt*, 1996; *Karato and Jung*, 1998; *Gaherty et al.*, 1999; *Hirth et al.*, 2000) or the presence of partial melt (*Anderson*, 1989), the lithosphere-asthenosphere boundary could occur over a much smaller depth range. Altogether, compared to the main seismic boundaries in the Earth (Moho, 410 km discontinuity, 660 km discontinuity, Core-Mantle-Boundary, boundary between the inner and outer core), the asthenosphere has very weak contrasts in seismic parameters to the surrounding intervals, and its detection requires high-resolution seismic data with a high signal-to-noise ratio (*Thybo*, 2006).

So far, the lithosphere-asthenosphere boundary has not been found globally, perhaps because of significant variations in the depth of the discontinuity (*Rychert et al.*, 2005). However, according to *Thybo* (2006), the upper mantle low velocity zone should be a global continental feature below relatively constant 100±20 km depth with the following characteristics:

- 1-5% lower velocity than in the surrounding intervals,
- strong attenuation of seismic waves, in particular S-waves,
- low electrical resistivity
- it includes seismic scatterers,
- its base is a seismic refractor at variable depth (the Lehmann discontinuity), which is shallow (150-250 km deep) in cold, stable areas and deep (250-400 km depth) in hot, active areas.

Thybo (2006) summarizes effects that may contribute to the creation of seismic low velocity zones, seismic scattering effects, and the origin of the Lehmann discontinuity at the base of the low velocity zone: rocks close to the solidus or in a partially molten state, the presence of fluids, change in anisotropy, change in rheology, metamorphic phase transformations, changes in composition, remnants of subducted slabs, an irregular base of the lithosphere, and magmatic intrusions. *Artemieva* (2003) suggests that in the East European Platform the low velocity zone formed by metasomatic processes as the result of

rifting processes. However, according to *Thybo* (2006) it is unlikely that this mechanism can explain its global occurrence.

Finally it has to be stated that there is still no consistent use of terms regarding discontinuities or gradients within the lithospheric mantle and between the lithosphere and mantle transition zone, which may lead to confusion and misunderstandings (see also *Anderson*, 1995).

In this chapter, observations of additional phases within *P* receiver function data are described first (section 6.2). These additional phases are interpreted to originate at converters in 50 and 65 km depth, respectively, and therefore are proposed to be a distinct feature of the lithospheric mantle beneath the western Bohemian Massif.

The *S* receiver function technique described in Chapter 4 enables observations of the lithosphere-asthenosphere boundary with a resolution so far only known for the Moho. The observations are described in section 6.3. Apart from the prominent signal of the Moho in the *S* receiver functions, a second deeper discontinuity with reversed polarity is observed in this study. Following earlier *S* receiver function studies mentioned above, the latter discontinuity is interpreted as the LAB, although it is not trivial to identify a seismic discontinuity with a mechanical or thermal boundary.

6.2 Additional phases observed in P receiver function data

Previous studies indicate the local existence of seismic reflectors and/or converters in the uppermost mantle at 50 to 60 km depth beneath the western Eger Rift as well as the Teplá-Barrandian and Moldanubian units (*Tomek et al.*, 1997; *Geissler et al.*, 2005; *Hrubcová et al.*, 2005). In the receiver functions obtained in this thesis, additional phases were observed in the area of Moho updoming and CO_2 gas emanations (western Eger Rift): a positive phase at about 6 s delay time with respect to the *P* onset, followed by a strong negative phase at about 7 to 8 s (in the following referred to as 7.5 s). Stations NALB and B24 in Figure 5.1 provide examples for the two additional phases; station NKC shows in the sum trace only the negative phase. The positive phase was already observed by *Geissler et al.* (2005) who named it the "*6 s phase*". To further investigate these phases, the area was divided into boxes (Figure 6.1). According to their piercing points at an interface of 65 km depth, the single receiver function traces were assigned to the boxes, corrected for moveout and stacked. Only sum traces obtained by at least ten single traces (grey boxes in Figure 6.1) were considered in the following. The boxes with additional phases at 6 s and/or 7.5 s are shaded pink. They form a coherent structure centred on the western Eger Rift. An overview over receiver function data of all boxes is given in Figure 6.2, which shows on top those boxes which contain a negative phase near 7.5 s and partly a positive phase near 6 s. Whereas the positive phase at 6 s occurs mainly in the central and eastern part of the pink shaded area, the negative phase occurs in all pink boxes. The pink area includes the area of CO_2 emanations (white ellipses in Figure 6.1), but also extends further to the north and south partly into the Regensburg-Leipzig-Rostock zone (see Figure 6.1). The area of apparent Moho updoming (see Figures 5.8 and 5.9) corresponds to the southwestern part of the pink shaded area.

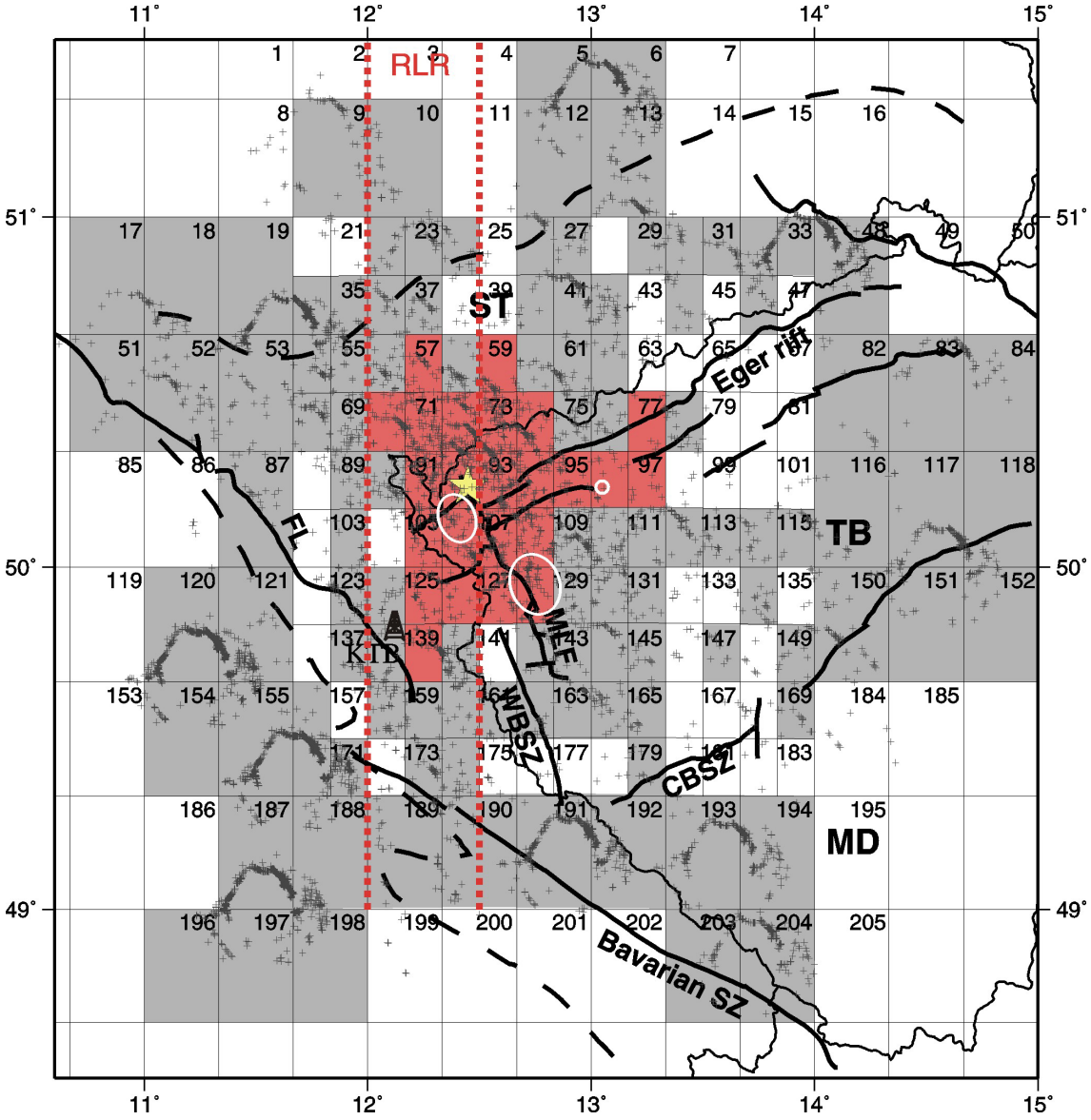

Figure 6.1: Occurrence of a negative phase near 7.5 s delay time. The piercing point of the rays at an interface at 65 km depth are shown by dark grey crosses. The area was divided into 205 boxes and only boxes with at least 10 individual traces were considered. Traces were stacked within each box. Pink boxes show an additional negative phase at 7.5 s, grey boxes do not. The yellow star shows the Nový Kostel main swarm earthquake area, white circles depict the main CO_2 degassing areas, RLR (red dotted lines) gives the approximate location of the Regensburg-Leipzig-Rostock zone (*Bankwitz et al.*, 2003).

6.3 Discussion: Structures within the lithospheric mantle

Figure 6.3 shows data along two profiles in which the additional phases are also shaded pink. The negative 7.5 s phase was not observed by *Geissler et al.* (2005), probably due to too sparse data. The observed additional phases could either be direct signals from structures in the upper mantle, or multiple reverberations from structures within the crust. A first step to test the difference between these two possibilities is an analysis of the distance moveout of the observed phases. For direct *Ps* conversions, the delay time of the

phase decreases with increasing epicentral distance, while for multiple reverberations it is opposite. Therefore, the receiver functions of four coherent boxes showing the additional phases near 6 and 7.5 s (boxes 93, 94, 107, 108, see Figure 6.1) were stacked within epicentral distance intervals of 10° (Figure 6.4). The delay time of the phases (Moho *Ps* conversion, phases at 6 and 7.5 s, crustal multiple *PpSs*/*PsPs*) was then measured for each epicentral distance interval. There is a weak trend visible that points to a decrease of delay time of the additional phases at 6 and 7.5 s with increasing epicentral distance, which indicates that they are direct converted phases from a structure in the uppermost mantle (Figure 6.4). However, the effects of moveout are very small in this shallow depth range. The differences are within the resolution limits of the data, therefore the obtained result is an indication rather than evidence. As expected, the crustal multiple *PpSs+PsPs* shows an increase in delay time with increasing epicentral distance. A test of different moveout corrections (for direct phases *Ps* and for the crustal multiple *PpPs*) furthermore shows that the amplitudes of both additional phases are slightly higher for the assumption of direct phases than for crustal multiple, which is a further indication for direct conversions rather than multiple reverberations. But again, the differences in amplitudes were very small and thus can not be taken for evidence.

To further test possible origins of these additional phases, synthetic receiver functions were calculated using the plane wave approximation described by *Kind et al.* (1995). *Geissler et al.* (2005) showed that the origin of the positive phase at 6 s could be in the crust or mantle or both (*Geissler et al.*, 2005). In seismic wide-angle data a reflector at 55 to 58 km depth was found by *Hrubcová et al.* (2005) which starts slightly SE of the western Eger Rift and runs SE into the central Moldanubian unit. In seismic reflection studies the reflector was also found (*Tomek et al.*, 1997). In the present study, the positive phase at 6 s is modelled by introducing a velocity increase at 50 km depth (Figure 6.5). However, in the BOHEMA data set this phase exists only in a subset of the pink boxes. The negative phase at 7.5 s could be modelled by assuming a velocity decrease of 3.7 ± 1.0 % at approximately 65 km depth in the uppermost mantle (Figure 6.5). A 5 km thick gradual velocity decrease between 65 and 70 km explains the data equally well. The velocity decrease can be interpreted as a local updoming of the lithosphere-asthenosphere boundary (LAB) beneath the western Eger Rift area. However, this proposed LAB would locally be significantly shallower than the 80 km depth proposed by *Babuška and Plomerová* (2001). In the area of the grey boxes, where the negative phase at 7.5 s is not observed, the LAB might be deeper and therefore its signal might be masked by crustal multiples. The relatively small amplitudes of the crustal multiples in the data traces at 12 s and 16 s compared to the computed traces can be attributed to several causes: (1) the decrease of the amplitudes of the multiples in the data trace due to not optimal stacking of the single traces as the moveout correction was performed for *Ps* and not for multiples, and (2) the missing effect of lateral crustal heterogeneities in the model (*Heuer et al.*, 2006).

An updoming of the LAB to 65 km depth could account for increased partial melt in the lithospheric mantle which may lead to the mantle-derived degassing of CO_2. The observed Moho updoming and proposed shallow LAB should induce an increased heat flow. However, it is not clear yet which contribution to the geothermal anomalies measured in the investigation area should be attributed to deeper-seated heat sources, because of the presence of radiogenic heat-producing granite complexes within the upper crust (see *Förster and Förster* (2000); *Emmermann and Lauterjung* (1997).

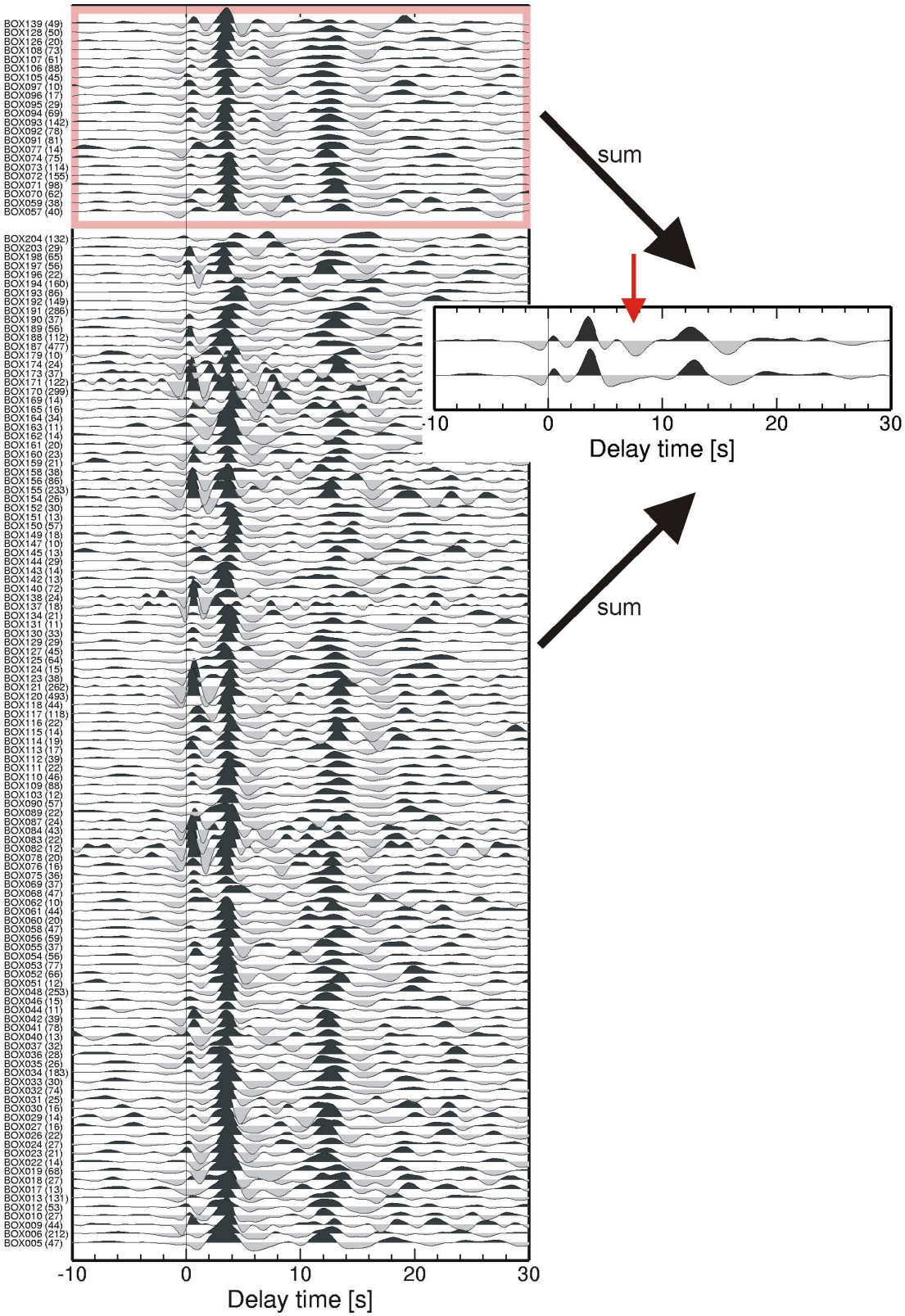

Figure 6.2: Sum traces of all boxes containing at least 10 individual traces (see Figure 6.1). Traces showing a negative phase near 7.5 s are displayed on top of the Figure. Some of them also show the positive phase near 6 s reported by *Geissler et al.* (2005). The traces in the lower part correspond to the grey boxes in Figure 6.1. To the right, the sum trace of all pink boxes (upper trace) and of all grey boxes (lower trace) of Figure 6.1 is shown. They are practically identical except for the time window between 6 and 10 s (red arrow points at observed negative phase).

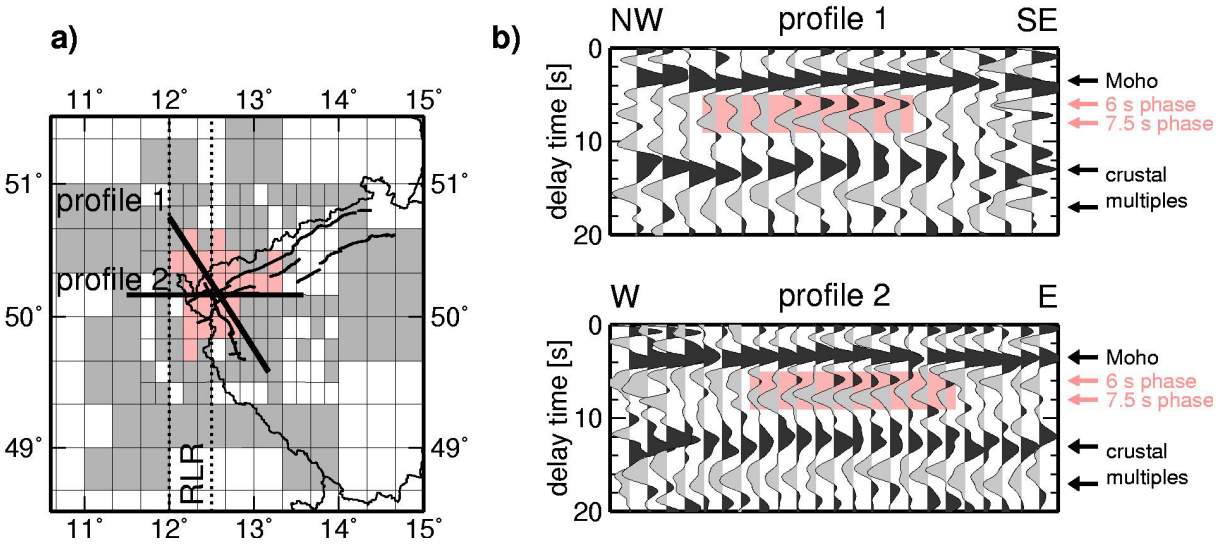

Figure 6.3: Sum traces of the boxes along two profiles in the time domain. **a)** location of the profiles. **b)** The profiles show the Moho Ps conversion at about 3.6 s. Positive/negative phases at about 6 s/7.5 s are shaded pink (*Heuer et al.*, 2006).

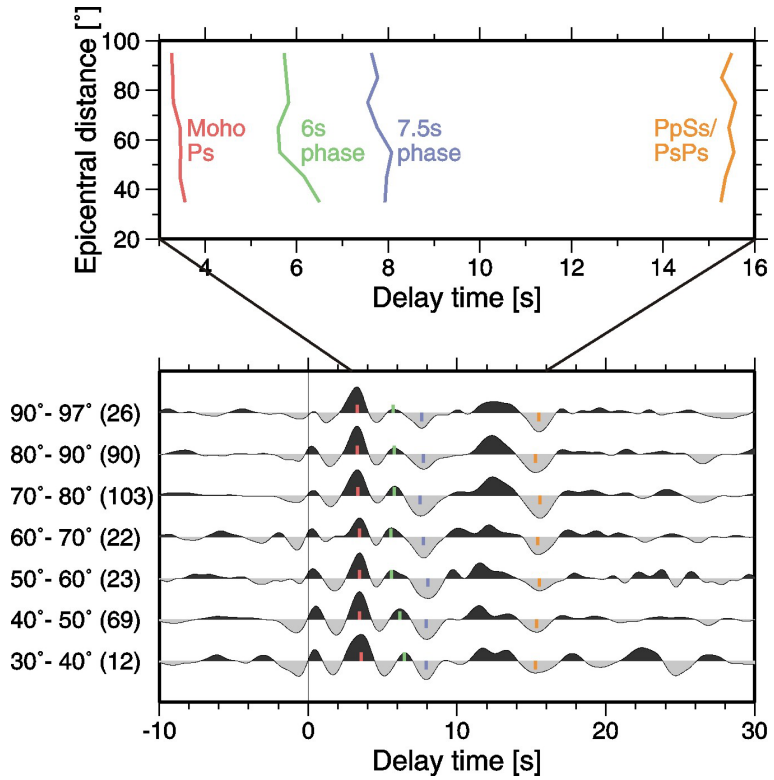

Figure 6.4: Test of the distance moveout of the additional phases near 6 and 7.5 s. Receiver functions of boxes 93, 94, 107, 108 were stacked within epicentral distance intervals of 10°. The stacked traces are shown in the lower part of the Figure. In brackets, the number of stacked individual traces is given. On top, the delay time axis is enlarged and delay times are drawn as lines to make trends better visible. The additional phases at 6 and 7.5 s show a slight decrease of delay time with increasing epicentral distance, which indicates that they might be direct conversions from a structure in the uppermost mantle rather than multiple reverberations from a structure within the crust.

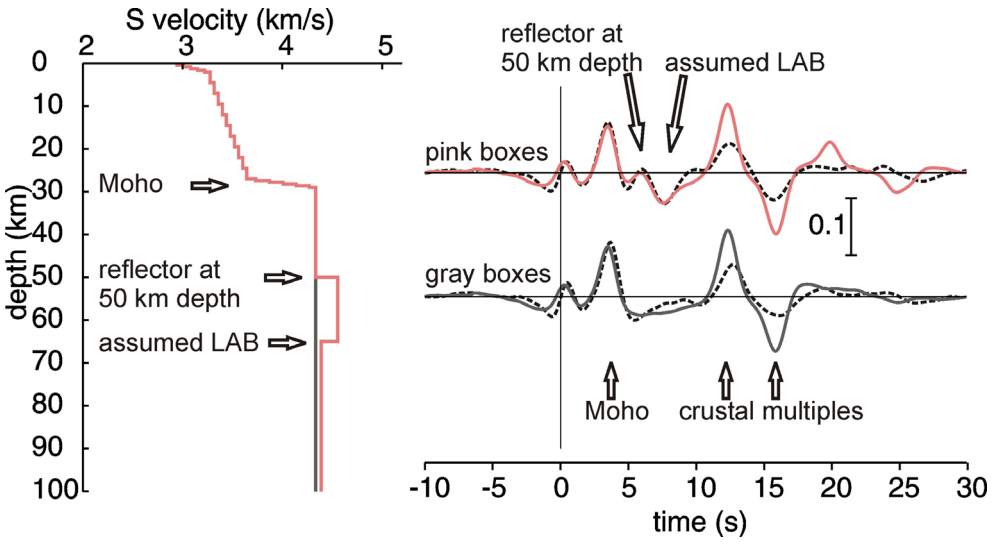

Figure 6.5: **Left:** Two models of S-wave velocity to explain the observed phases in the grey and pink boxes (*Heuer et al.*, 2006). The models are identical down to a depth of 50 km. **Right:** Black dashed line shows the stacked signal of all traces within the pink boxes (top) and grey boxes (bottom). The traces are practically identical except for the phases at 6 s and 7.5 s, interpreted as „reflector at 50 km depth" and „assumed LAB", respectively. Amplitudes of the additional phases at 6 s and 7.5 s in the data of the pink boxes are small due to suboptimal stacking of the traces as the delay time of the phases is not exactly the same and the phase at 6 s occurs only in a subset of the pink boxes. The solid line shows the response of the S velocity model on the left. The scale shows the amplitudes in per cent of the incoming P-wave.

An updoming of the LAB should be reproducable by the method of *S* receiver function analysis (see Chapter 4). Thus, *S* receiver function investigation of the data can help to deny or confirm the existence of a possible LAB updoming suggested by the data of *P* receiver functions. This is shown in the next section.

6.4 Observations in S receiver function data

6.4.1 *S* receiver functions obtained at the seismic stations

For 80 stations of the BOHEMA experiment and the experiment by *Geissler et al.* (2005) (see Appendices A.1 and A.2), *S* receiver functions were computed as described in Chapter 4. Examples of *S* receiver functions obtained at four stations are shown in Figures 6.6 and 6.7. At 3-4 s delay time after the *S* onset, the strong signal of the Moho *Sp* conversion can be seen. At about 10 to 12 s, a weaker negative phase is observed. Following the current state of research (e.g. *Li et al.,* 2004 ; *Kumar et al.,* 2005a, 2005b, 2006; *Sodoudi et al.,* 2006a,b), this negative phase is attributed to the lithosphere-asthenosphere boundary which has a negative velocity gradient.

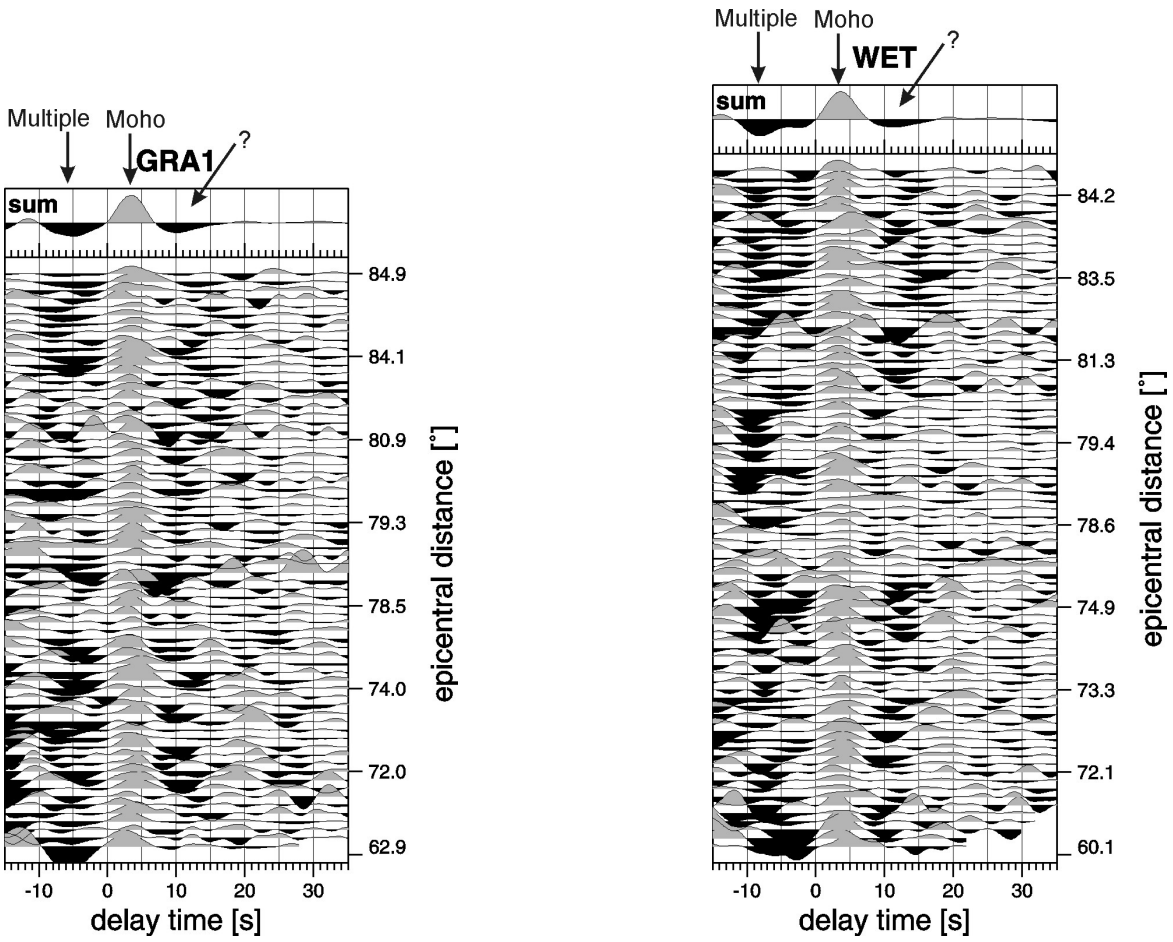

Figure 6.6: *S* receiver functions obtained for permanent stations GRA1 (left) and WET (right) of the German Regional Seismic Network. The delay time of the seismic signals with respect to the time of the *S* onset is shown. Each trace shows the *S* receiver function of a single teleseismic event. A low pass filter of 4 s and moveout correction were applied. The traces are sorted by the epicentral distance of the corresponding event. Note that the scale of epicentral distances is not linear. On top of the Figure, the sum traces of the single traces are shown for each station. At about 3-4 s delay time, the signal of the Moho *Sp* conversion can be seen. At about 10 to 12 s, a negative signal is observed. The signals occurring at negative delay times are attributed to multiple reflections.

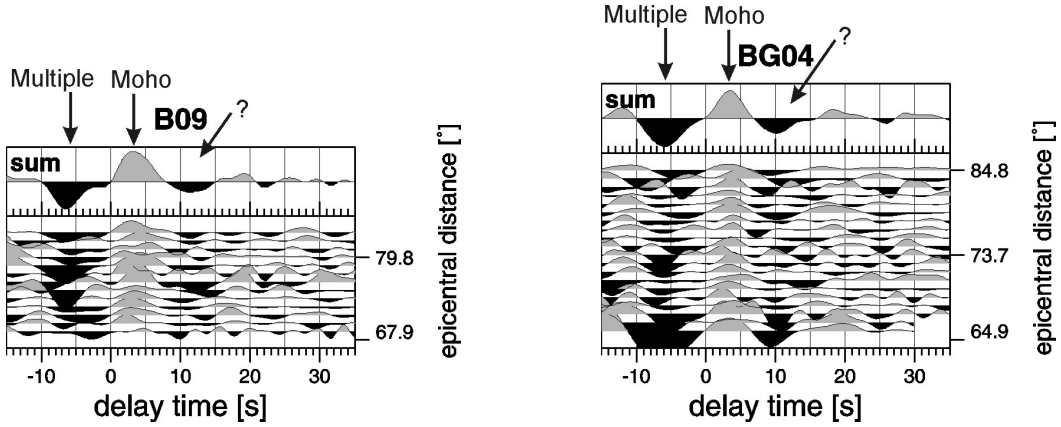

Figure 6.7: *S* receiver functions obtained for temporary stations B09 (left) and BG04 (right) of the BOHEMA network. Description see Figure 6.6.

6.4.2 Dividing the data into local "boxes"

For investigating the lithosphere-asthenosphere transition with *S* receiver functions it is important to consider the location of origin of the negative phase. Due to the ray geometry, the piercing point of a ray at an interface at 80 km depth is situated approximately 70-155 km away from the station for epicentral distances of 85-60°, respectively. If the station locations are as close to each other as in this study, the piercing points of different stations strongly overlap. Hence the data must be grouped according to their piercing points at a certain depth rather than stationwise. A map of the piercing points at 80 km depth for the

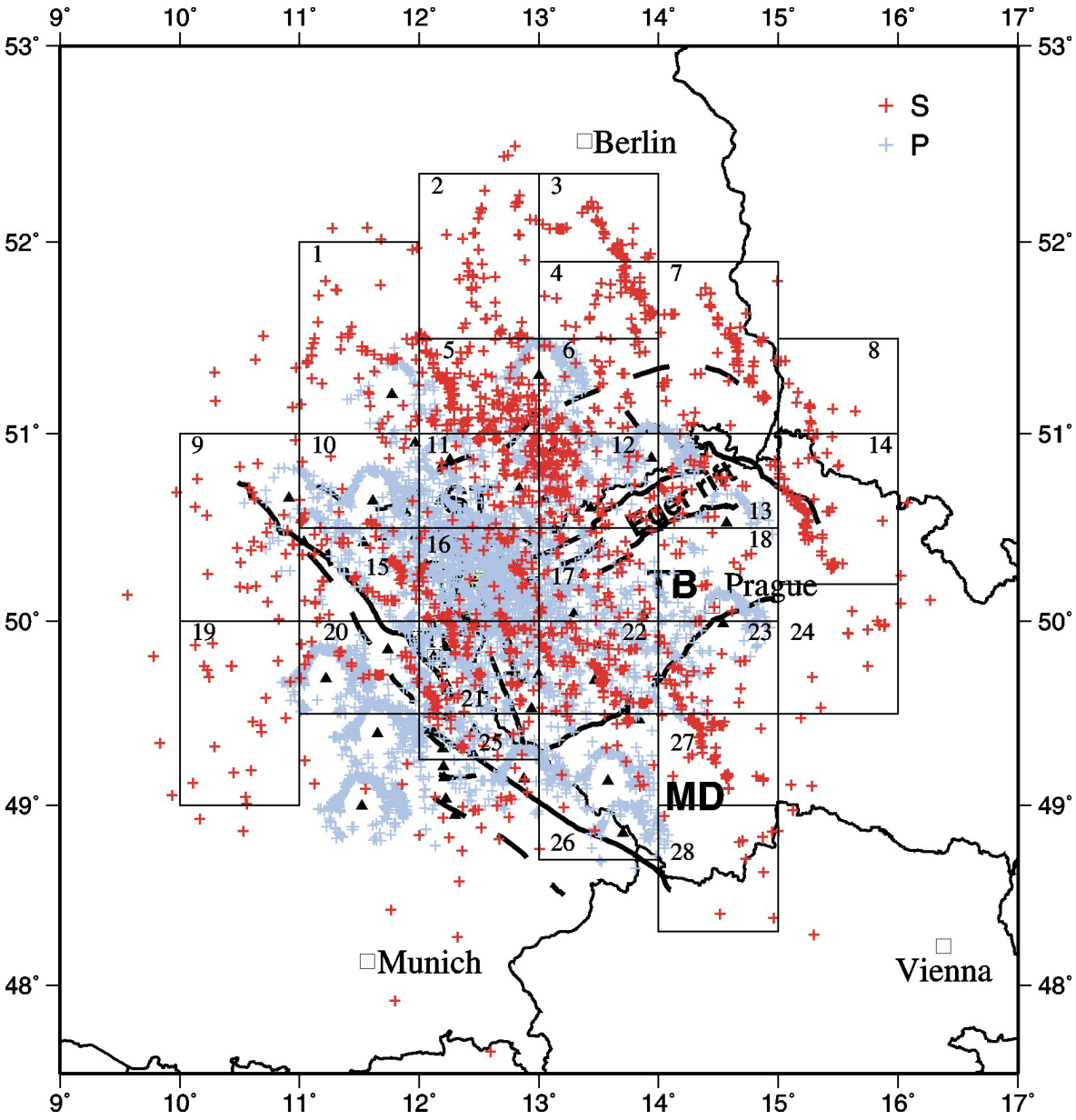

Figure 6.8: Piercing points of *P* (blue crosses) and *S* (red crosses) rays at an interface at 80 km depth. Seismic stations are shown by black triangles. For *S* receiver functions, the piercing points are located approximately 70 to 155 km away from the recording station. As the piercing points of different stations overlap each other, the area was divided into 28 boxes to group the *S* receiver function data geographically for further investigations.

obtained *S* receiver functions compared to piercing points at 80 km depth for *P* receiver functions is shown in Figure 6.8.

The area was then divided into 28 non-overlapping boxes also shown in Figure 6.8. The width of the boxes is 1° longitude and between 0.4 and 1° latitude, which corresponds to box sizes of approximately 70 km E-W and 45-112 km N-S extension (3200 km^2 to 8000 $km^{2)}$ at the Earth's surface. Only box 25 is smaller.

The single traces of each box were visually checked for quality. As the delay time of the Moho onset is known from *P* receiver functions to occur around 3 to 4 s, an approximate delay time of 2 to 5 s of the Moho *Sp* conversion signal was one quality criterion. Furthermore, extremely noisy traces were also omitted. Finally, the traces were stacked to improve the signal-to-noise ratio. Examples for *S* receiver functions obtained for individual boxes are shown in Figure 6.9. Like in the examples for individual stations, the Moho *Sp* conversion at 3 to 4 s delay time is very strong and clear. It is followed by a weaker negative signal at 8 to 14 s attributed to the lithosphere-asthenosphere transition. This negative signal does not always seem to be coherent in the individual traces at one station, probably due to scattering of the phase.

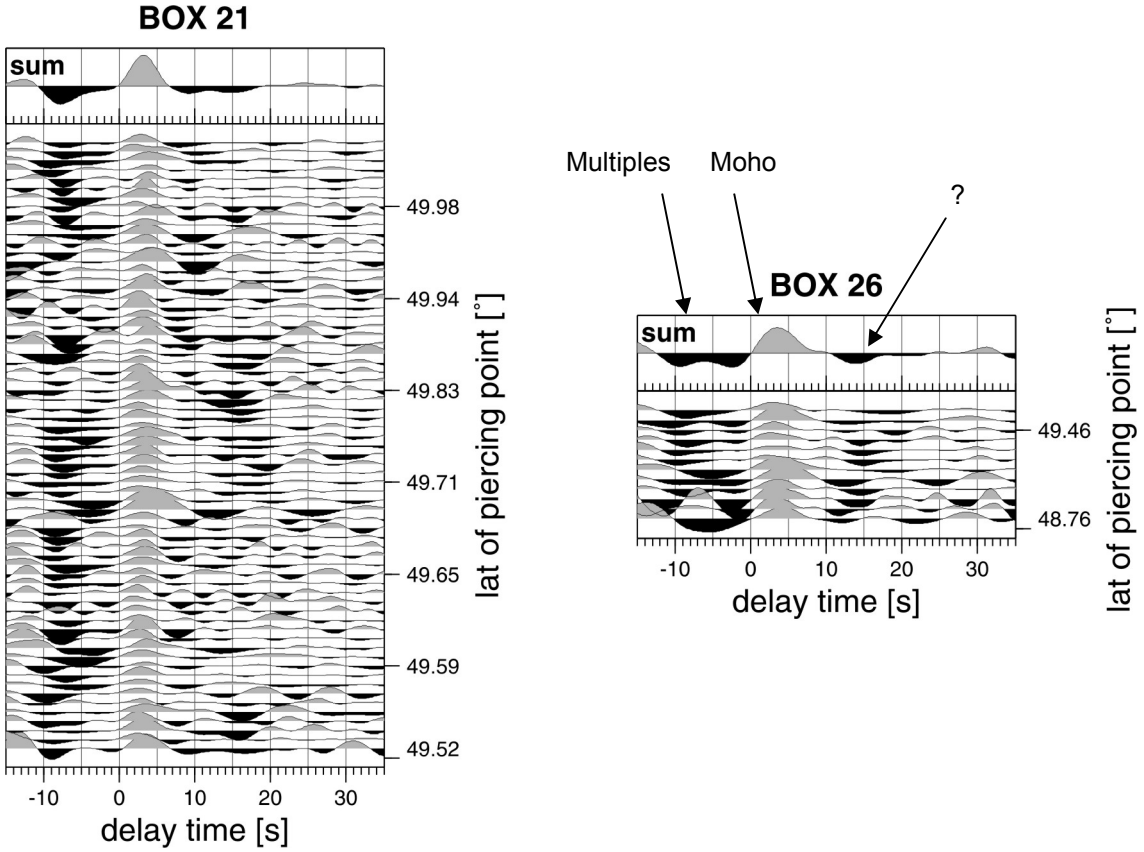

Figure 6.9: Data examples of *S* receiver functions obtained for six boxes. Zero time is the *S* arrival time. The processing of the traces was carried out in the same manner as described in Figure 6.6, only that here the traces are sorted by the latitude of the piercing points at 80 km depth. Note that the scale of latitude of piercing point is not linear. Again, on top of the Figure the sum traces of the single traces are shown for each box **(continued on next page)**.

Figure 6.9, continued.

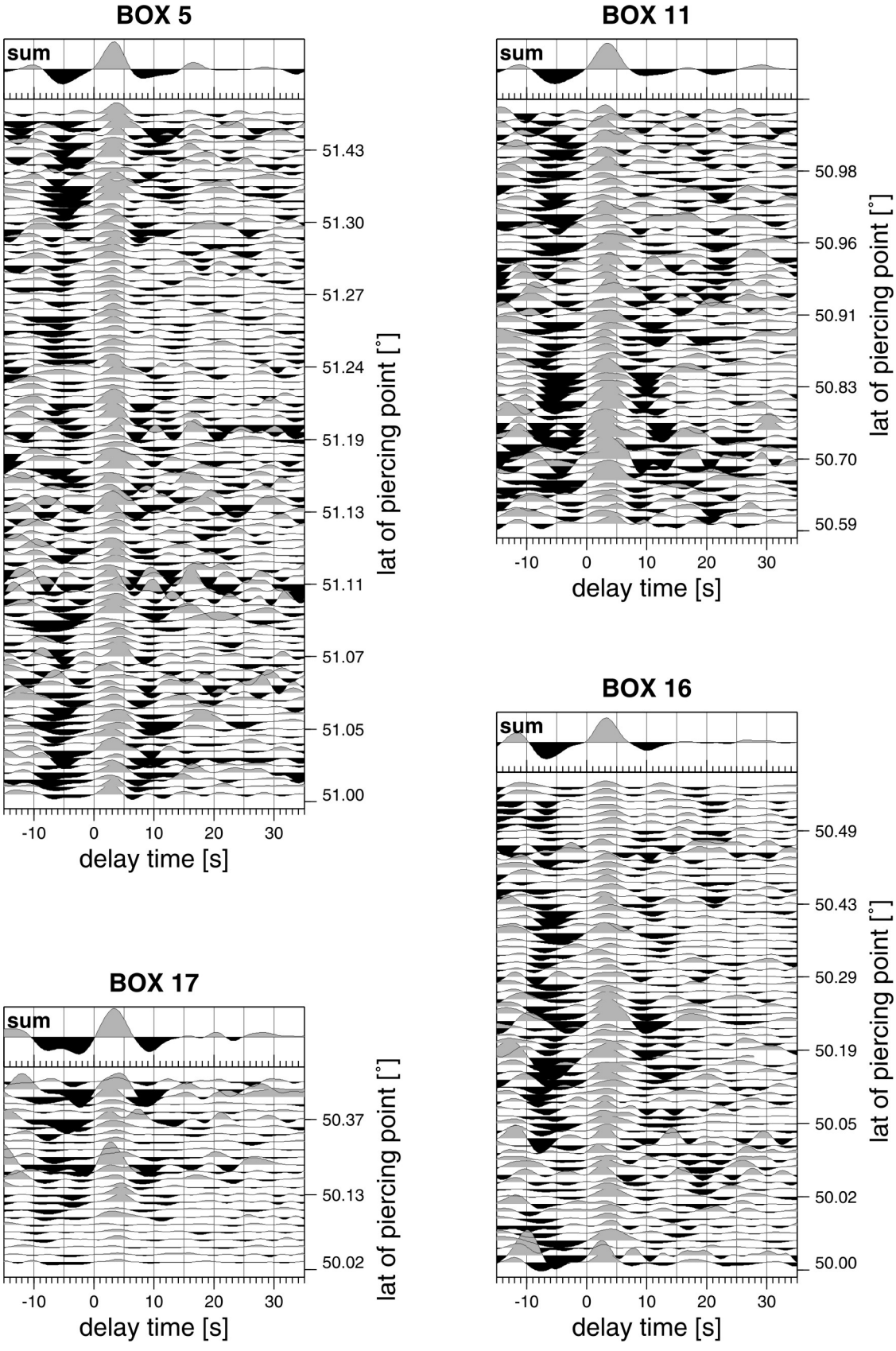

Figure 6.10a shows the summation traces of all 28 boxes sorted by box number. After the Moho signal at 3 to 4 s delay time, the negative phases arrive at 8 to 14 s. They are coherent for most boxes and clearly arrive later in boxes 25 to 28 (at 12 to 14 s versus 8 to 10 s in boxes1 to 24). As the signal is rather weak and for most boxes arrives directly after the Moho *Sp* conversion signal, there is also the possibility of it being merely a side lobe of the Moho signal and thus an artefact produced by the deconvolution. This would be the case if the *Q* component also showed such side lobes in the deconvolved *S* signal. To investigate this, the *Q* components were stacked for each box in order to compare the sum traces of the *Q* components with those of the *L* components (the *S* receiver functions). This is shown in Figure 6.10(b). The comparison shows that there are no or only very weak side lobes in the *Q* summation traces. Therefore it can be excluded that the negative signals observed in the *S* receiver functions at 8 to 14 s are only artefacts of deconvolution but are most probably the *S*-to-*P* conversions generated at the negative velocity gradient of the lithosphere-asthenosphere transition.

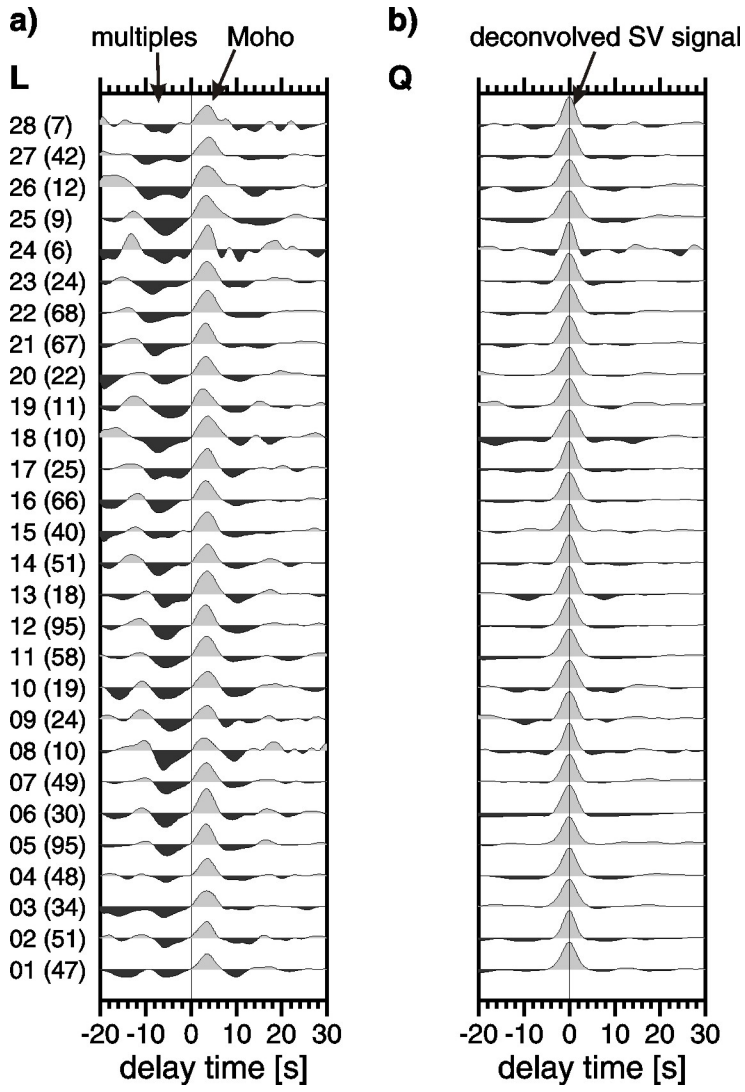

Figure 6.10: Comparison of summation traces of *L* and *Q* components for all boxes. On the left, box numbers and, in brackets, the number of stacked traces are shown.
(a) *S* receiver functions (*L* components) show a very strong and clear Moho *Sp* signal at 3 to 4 s delay time The negative signal attributed to the lithosphere-asthenosphere transition follows at approximately 8 to 14 s and is weaker, but still coherent for most boxes. In boxes 25 to 28, the negative signal clearly arrives later than in the other boxes (at 12 to 14 s).
(b) The *Q* components show no or only weak side lobes in the deconvolved *S* signal, so that it can be excluded that the negative phases observed before and after the Moho *Sp* conversion signal are merely artefacts generated by deconvolution. Instead, the negative phase at around 10 s delay time is most likely the conversion signal from the lithosphere-asthenosphere transition.

6.5 Discussion

6.5.1 Lithospheric thickness beneath the western Bohemian Massif

The boxes that show an unambiguous negative conversion signal after the Moho *Sp* conversion are shown in Figure 6.11 together with the delay time that was picked for the negative phase. For some boxes (boxes 2-5, 9, 21-23, see Figure 6.10) the negative signal in the sum trace was either doubled or very broad, so that no clear decision for a certain delay time of the signal could be made.

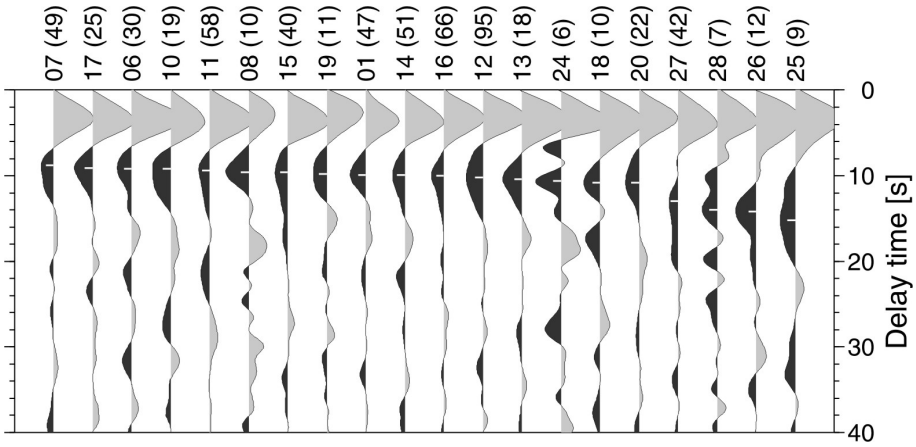

Figure 6.11: Boxes for which an unambiguous delay time of the negative phase could be picked (small black dashes). The boxes are sorted by increasing delay time of the negative phase.

A good approximation of the depth origin of the negative phase can be achieved by multiplying the picked delay time by a factor of 9 based on the IASP91 standard earth model (*Kennett and Engdahl, 1991*). The result of this depth estimation is visualized in the map in Figure 6.12. According to the current state of knowledge, this negative phase is usually interpreted as the conversion from the lithosphere-asthenosphere transition. However, this transition is not very well constrained yet regarding its nature, depth location and width of gradient zone. If it is interpreted as the lithosphere-asthenosphere transition, the map in Figure 6.12 shows lithospheric thickness of 80 to 90 km beneath the Saxothuringian and partly the Teplá-Barrandian unit. Towards the south, the thickness first seems to slightly increase (boxes 20, 18, 24: 95 km) and then strongly increases in the Moldanubian part of the investigation area to 115 to 135 km. Boxes 24, 25 and 28 in the very south show only a scarce data coverage. However, as the obtained depth values of the boxes in the Moldanubian part are quite coherent, the result of a thick lithosphere in this area is considered to be reliable. The obtained values are summarized in table 6.1.

It is interesting to note that the boxes in the transition from the Saxothuringian/Teplá-Barrandian type lithosphere to the thicker Moldanubian lithosphere (boxes 21 to 23) belong to the boxes where it was difficult to determine a clear negative signal in the summation trace. Especially for boxes 21 and 22 a doubling or broadening of the negative signal can be stated which could point to either an abrupt increase of lithospheric thickness

or a very steep slope or possibly even a structure from palaeosubduction within the lithosphere in the mentioned boxes. *Babuška and Plomerová* (2001) observed in the area of box 21 a mixture of anisotropic characteristics of the Saxothuringian and Moldanubian units within the lower lithosphere south of the surface trace of the Saxothuringian/Moldanubian contact. As an explanation the authors suggested underthrusting of a part of the Saxothuringian subcrustal lithosphere beneath the Moldanubian or a hypothetical remnant of the Early Palaeozoic oceanic lithosphere subducted to the south during collision of the Saxothuringian and Moldanubian units.

Table 6.1: Box number, coordinates of the centre of the box, number of traces n stacked within each box, measured delay time of the *Sp* conversion from the LAB and corresponding calculated LAB depth.

Box №	lon [°E]	lat [°N]	n	delay time LAB [s]	depth LAB [km]
1	11.5	51.5	47	9.9	90
2	12.5	51.925	51	?	?
3	13.5	52.125	34	?	?
4	13.5	51.7	48	?	?
5	12.5	51.25	95	?	?
6	13.5	51.25	30	9.2	85
7	14.5	51.45	49	8.8	80
8	15.5	51.25	10	9.6	85
9	10.5	50.5	24	?	?
10	11.5	50.75	19	9.2	85
11	12.5	50.75	58	9.4	85
12	13.5	50.75	95	10.2	90
13	14.5	50.75	18	10.4	95
14	15.5	50.6	51	9.9	90
15	11.5	50.25	40	9.6	85
16	12.5	50.25	66	10.0	90
17	13.5	50.25	25	9.1	80
18	14.5	50.25	10	10.8	95
19	10.5	49.5	11	9.8	90
20	11.5	49.75	22	10.8	95
21	12.5	49.75	67	?	?
22	13.5	49.75	68	?	?
23	14.5	49.75	24	?	?
24	15.5	49.85	6	10.6	95
25	12.5	49.375	9	15.2	135
26	13.5	49.1	12	14.2	130
27	14.5	49.25	42	13.0	115
28	14.5	48.75	7	14.0	125

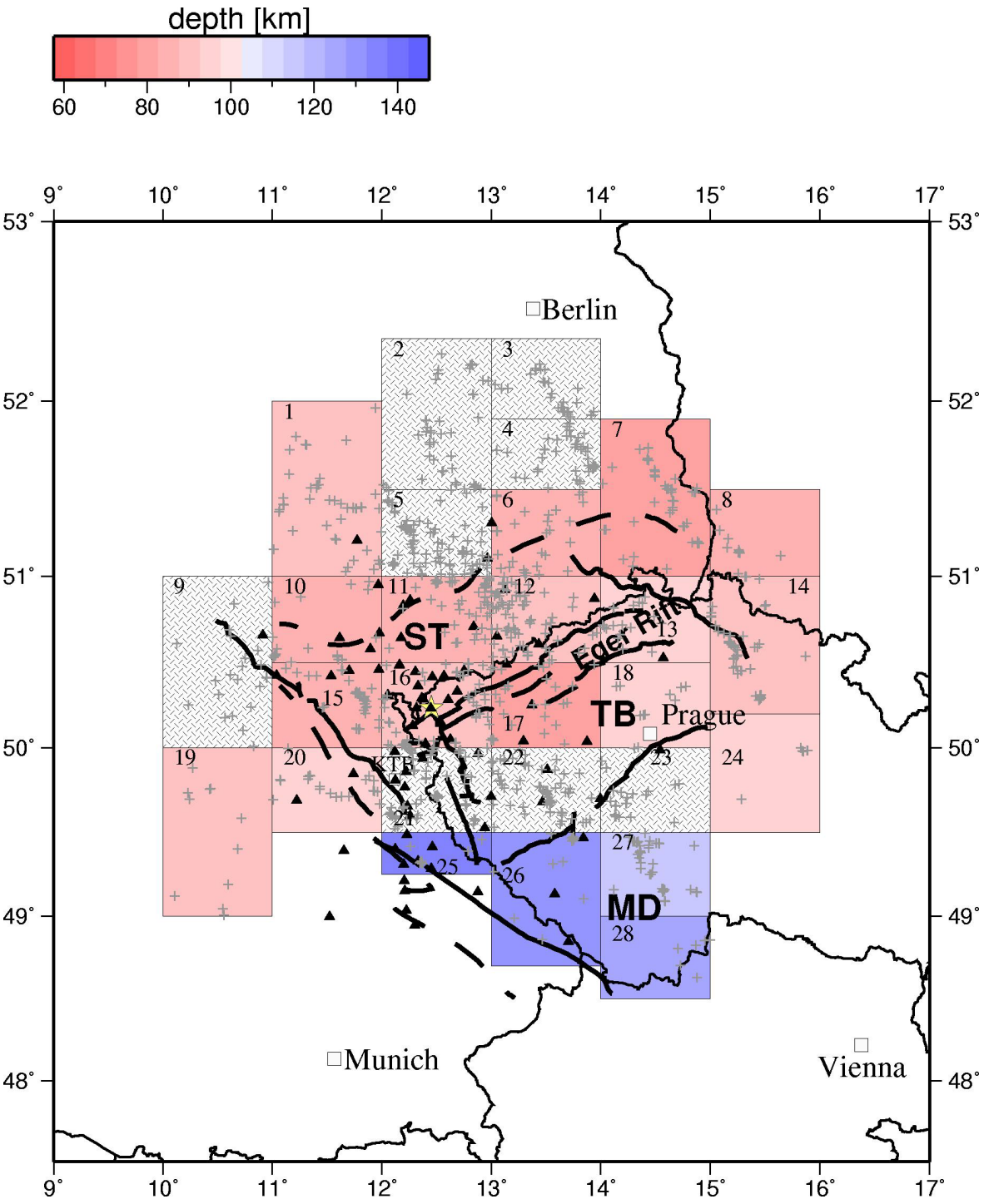

Figure 6.12: Map of the depth origin of the negative phase, which probably represents the lithosphere-asthenosphere transition beneath the western Bohemian Massif. The grey crosses show the data coverage of the boxes – the crosses correspond to piercing points of the rays at 80 km depth. In the Saxothuringian and partly the Teplá-Barrandian unit the depth is 80 to 90 km, in the Moldanubian part of the investigation area it is 115 to 135 km. In the hatched boxes, the negative signal of the lithosphere-asthenosphere transition was either ambiguous or too broad for determining a clear peak.

6.5.2 N-S and E-W Profiles

Figures 6.13-6.18 show three N-S and three E-W profiles of *S* receiver functions (single traces and stacked traces) in the investigation area. They will be discussed in the following.

The N-S profile between 12°-13°E (Figure 6.13) indicates in most parts a lithospheric thickness of approximately 80 to 90 km. North of 51°N, the negative signal is ambiguous both in the single and stacked traces. Nevertheless, north of 51.7°N the amplitudes of a slightly south dipping LAB seem to be quite strong. This is not visible in the map in Figure 6.13, because all traces between 51.5-52.5°N lie within box 2, which in the sum trace gives not such a clear image of a deep LAB but shows a rather broad signal (see Figure 6.10a). South of 50°N the LAB clearly becomes deeper both in the single and stacked traces with delay times around 13 s to more than 15 s, corresponding to LAB depths of 120 to 140 km. The origin of a negative signal at approximately 22 s delay time between 50.5 and 51.2°N is not clear. It could be caused by a downward decrease in seismic velocities in approximately 200 km depth.

The N-S profile between 13°-14°E (Figure 6.14) shows a clear and smooth LAB between 50°-51.5°E at ca. 90 km depth in the single and stacked traces. South of 50.2°N, the LAB again clearly deepens down to 120 to 130 km like in the profile east of it. North of 51.5°N there is generally no clear negative signal visible at the expected LAB delay time both in the single and stacked traces. This is contrary to the profile between 12°-13°E. Only the northernmost trace at about 52.2°N shows a strong negative signal at 12 s delay time.

The third N-S profile between 14°-15°E (Figure 6.15) shows a clear and relatively even LAB signal from about 50.0°N northwards. Between 49.3°-49.8°N there is a small, very shallow negative signal at approximately 7 s delay time, corresponding to a depth of origin of approximately 65 km depth. The origin of this very shallow signal is not clear. In the southern part of the profile (south of 49.3°N), the delay time of the negative signal is not very clear both in the single traces and in the stacked traces. This is probably due to sparse data. However, the adjacent Alpine orogen may also be a cause of the more complicated structure in the south of this profile. The negative signal at about 13 s delay time is interpreted as the LAB signal in the southern part of the profile so that it is coherent with the other N-S profiles. In this profile, the time interval later than 15 s delay time is rather noisy even in the stacked traces. As the data is not very dense, the seemingly coherent structures within later (deeper) parts of the profile should not be overinterpreted.

The southernmost E-W profile, which runs between 49.5°-50.0°N (Figure 6.16), shows in its western part a LAB depth of approximately 100 km. Between about 12.3°-14°E it clearly deepens with a maximum of approximately 135 km depth at 12.7°E. Between 13°-14°E there seems to be a doubling of the negative signal, but as the corresponding N-S profile (Figure 6.14) shows a rather clear phase at 13 to 14 s, the LAB signal in this profile is interpreted accordingly to originate at a depth of 120 to 130 km. The trace with the very shallow negative signal 14.4°E obviously corresponds to the unusually shallow signals observed in the N-S profile between 14-15° (Figure 6.15). The explanation of this signal is not clear yet.

The E-W profile between 50.0°-50.5°N (Figure 6.17) shows in the west up to 12.0°E a 80-90 km deep LAB. At about 12.3°E, the LAB signal is shallower (7 s delay time, corresponding to approximately 65 km depth) and deepens again slightly towards the east

up to about 90 km. A doubling of the negative signal is observed from 13.7°E eastwards which is also observed in the corresponding N-S profile between 14-15°E (Figure 6.15). Although the data is rather sparse in this part of the profile, the doubling is coherent among four (partly overlapping) stacked traces .

The northernmost E-W profile between 50.5°-51.0°N (Figure 6.18) shows a strong and even LAB signal at approximately 90 to 100 km depth.

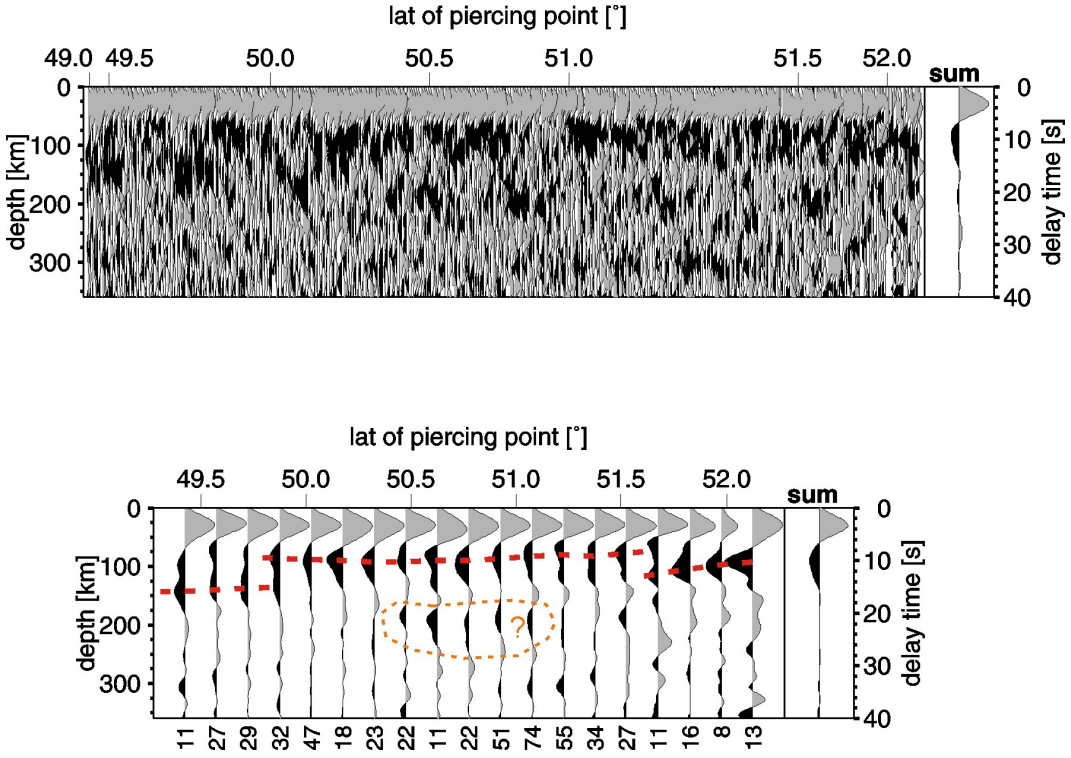

Figure 6.13: N-S profiles of *S* receiver function data between 12°-13°E. In the upper profile, single traces sorted by latitude of their piercing point at 80 km depth are shown with even trace spacing. Thus, the ordinate showing the latitude of the piercing points is not linear. On the right side, the sum trace of all single traces is shown. The right ordinate gives the delay time relative to the S onset, the left ordinate shows the approximate corresponding depth. Single traces are filtered with a 6 s low pass filter. In the lower profile, the single traces are stacked within moving geographical windows of 0.25° latitude and 0.1° overlap. Here, the ordinate showing the latitude of piercing points is linear. The stacking process enhances the stable signals while it suppresses some of the noise of the single traces. The stacked traces are filtered with a 4 s low pass filter. Below the stacked traces, the number of individual traces used for stacking is given.

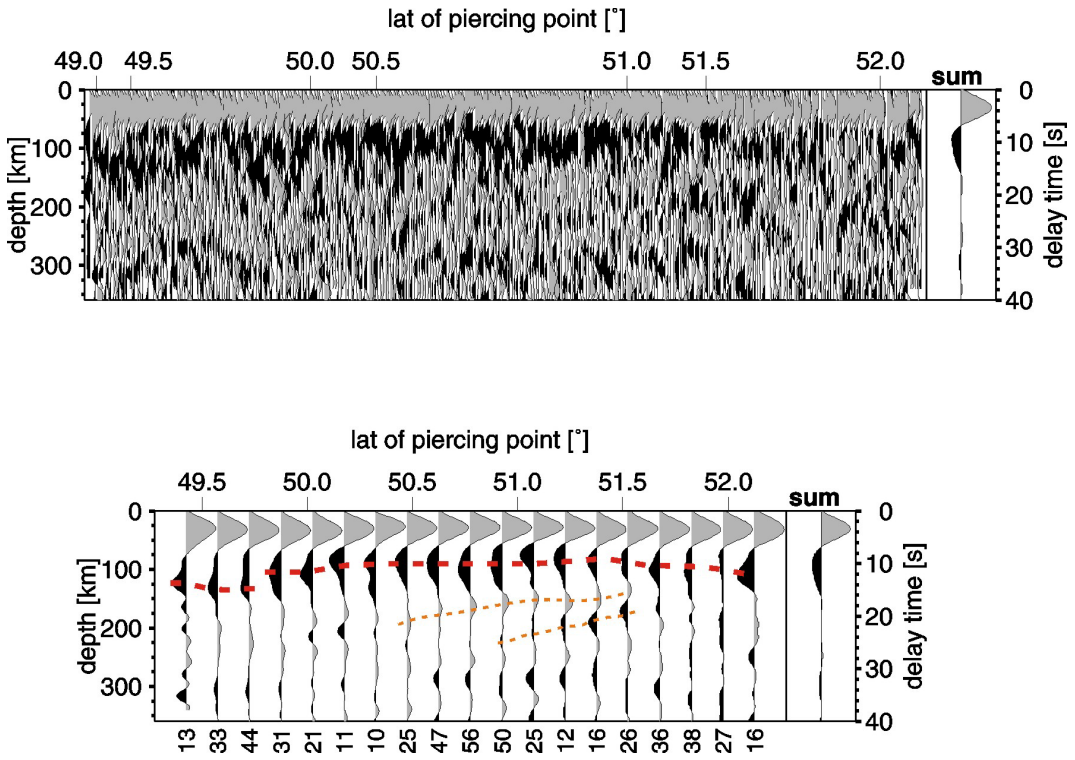

Figure 6.14: N-S profiles of *S* receiver functions between 13°-14°E. Description see Figure 6.13.

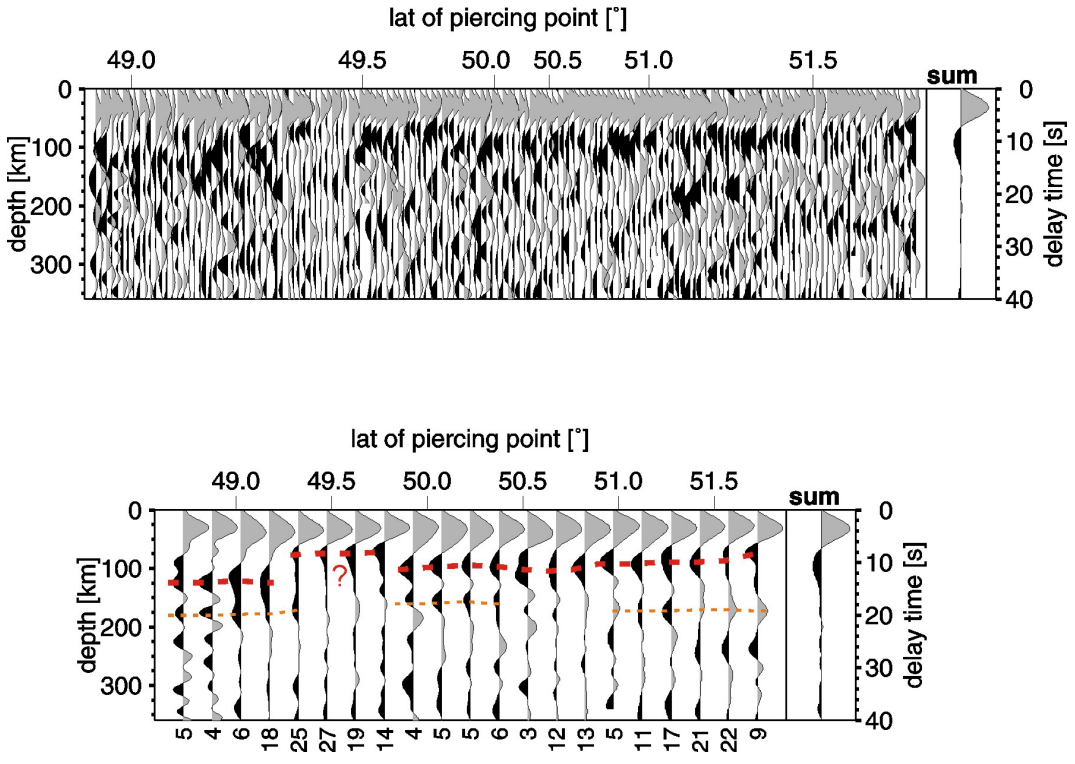

Figure 6.15: N-S profiles of *S* receiver functions between 14°-15°E. Description see Figure 6.13.

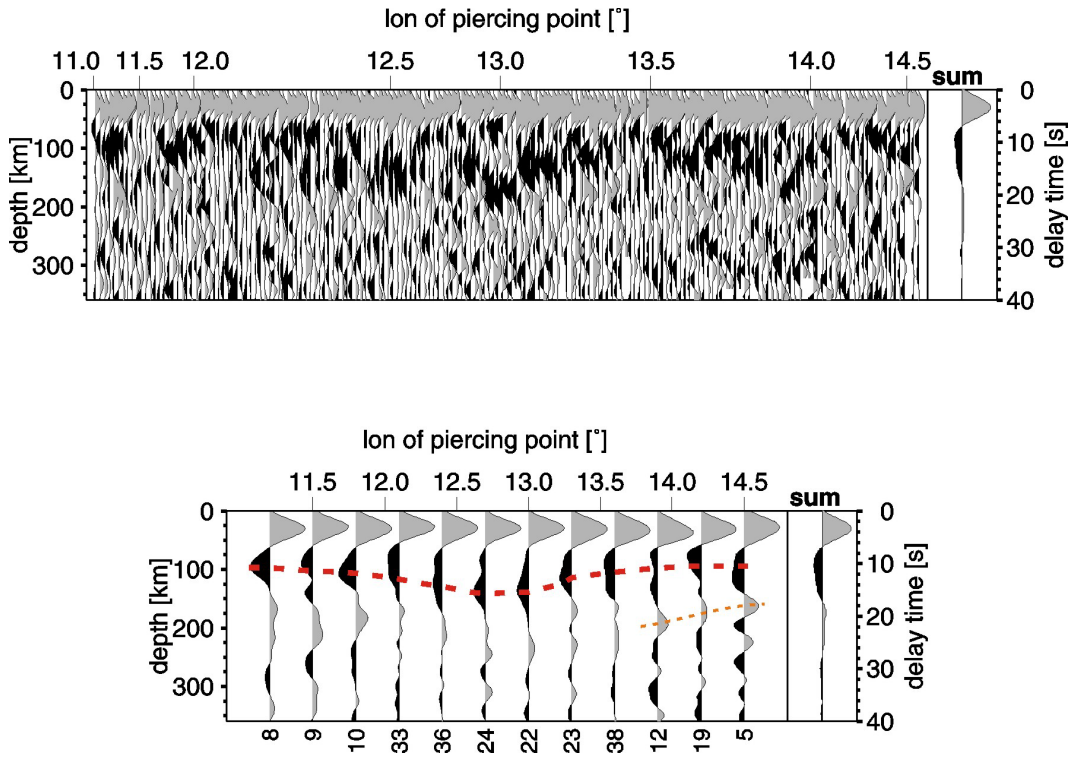

Figure 6.16: E-W profiles of *S* receiver functions between 49.5°-50.0°N. Description like Figure 6.13, but for E-W profiles the single traces were stacked within moving geographical windows of 0.3° longitude with an overlap of 0.1°.

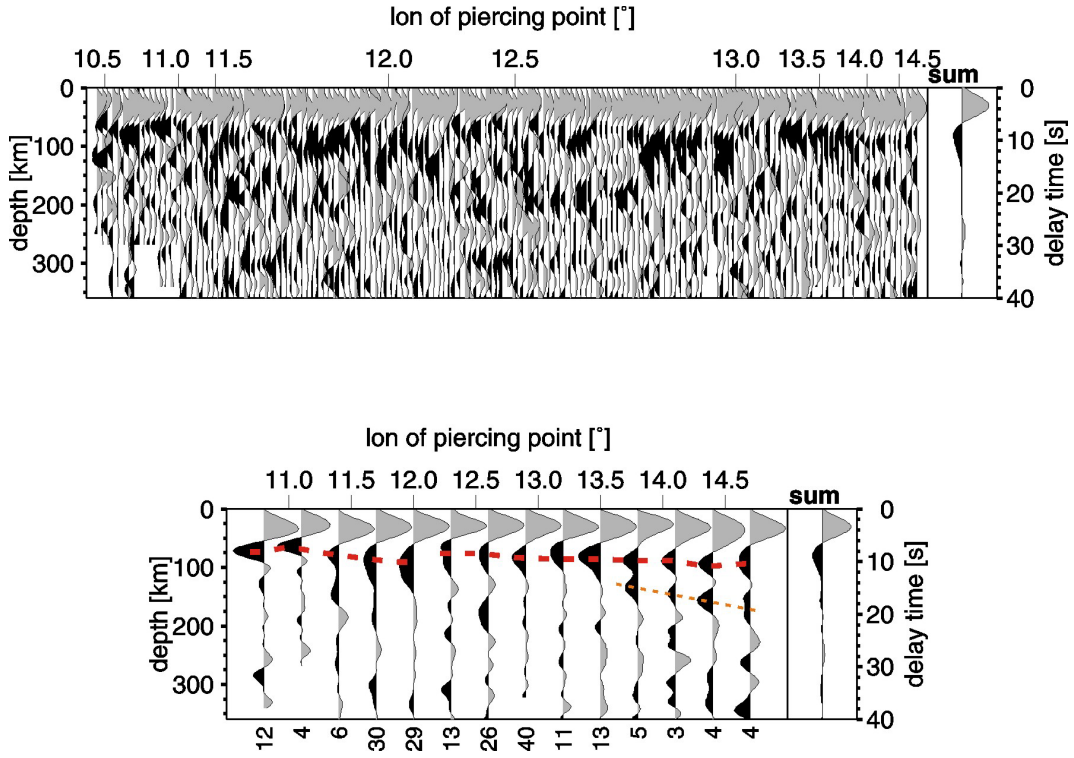

Figure 6.17: E-W profiles of *S* receiver functions between 50.0°-50.5°N. Description see Figure 6.16.

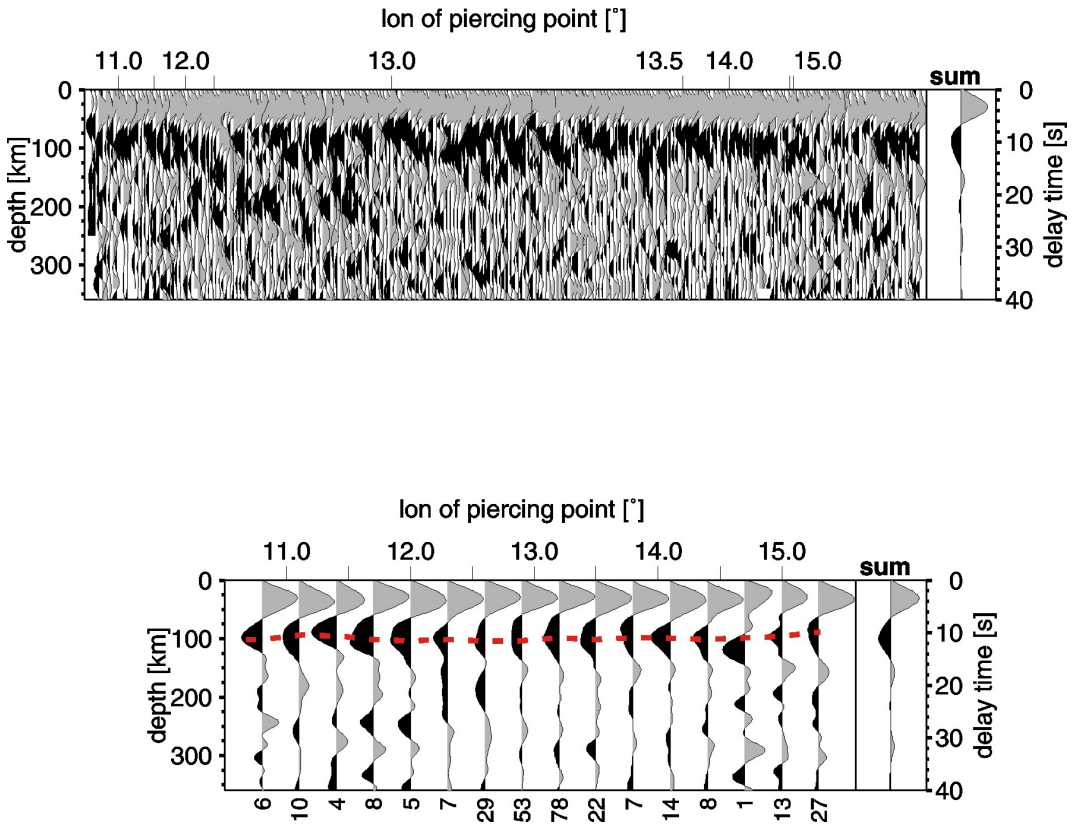

Figure 6.18: E-W profiles of *S* receiver functions 50.5°-51.0°N. Description see Figure 6.16.

Figure 6.19 shows the location of the N-S profile between 12°-13°E again, as it will be further discussed in the following. In Figure 6.20, data of *P* and *S* receiver functions are directly compared. The *S* receiver function profile has already been described above. The *P* receiver functions show a much sharper and better resolved Moho signal at 3.5 s due to their higher frequency content. At approximately 12 and 16 s the strong and coherent crustal multiples appear. In most of the stacked *P* receiver function traces of the profile the negative signal after the Moho *Ps* conversion splits into several peaks and can not be clearly identified. Only in the latitude interval of 49.9° to 50.6° the negative conversion is very clear and unambiguous. No indications for structures in the crust that might cause this negative phase are visible in the data. This area corresponds to the area of pink boxes. However, the positive phase near 6 s delay time does not show in the data, probably because it occurs only in a smaller area than the negative phase near 7.5 s.

By comparing the sum traces of the *P* receiver functions with the sum trace of the *S* receiver functions, it is not clear whether the negative signal observed at about 7.5 to 8 s in the P receiver functions corresponds to the negative signal in the *S* receiver functions at about 9 to 10.2 s interpreted as the conversion from the LAB. The superimposed traces of *P* and *S* receiver functions in Figure 6.21 show that in the *S* receiver functions the negative signal occurs about 2 s later than in the *P* receiver functions. The difference of 2 s in the delay times is significant as the stacking of individual traces provides rather stable phases. Furthermore, the value is clearly above the estimated uncertainty of 0.2 s for picking delay times in the receiver function traces.

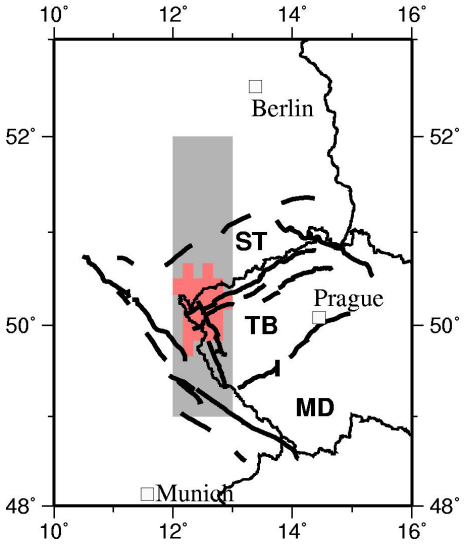

Figure 6.19: The grey shaded band between 12 and 13°E shows the location of the data profiles of Figures 6.20 and 6.21. The red area within the profile corresponds to the area where a negative phase at about 7.5 s delay time and partly a positive phase near 6 s delay time occurs in the *P* receiver functions (see Figure 6.1).

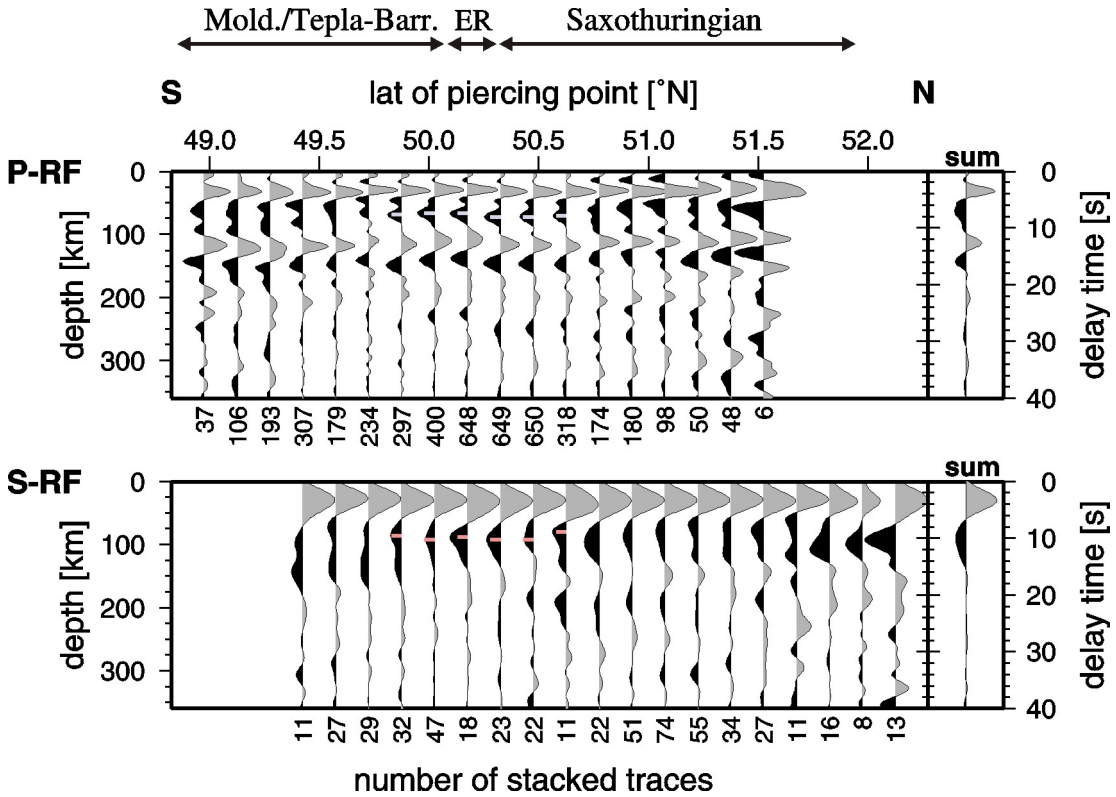

Figure 6.20: Comparison of *P* and *S* receiver functions along the N-S profile between 12°-13°E. Top: *P* receiver functions, stacked in windows of 0.25° latitude with 0.1° overlap and filtered between 2-20 s. Bottom: *S* receiver functions stacked and filtered in the same manner as P receiver functions. To the right of each profile, the sum trace of all individual traces is shown. The individual traces were sorted before-hand according to their piercing points in 80 km depth. The maxima of the negative phase after the Moho signal were picked in the area of interest between 49.9°-50.6°N. In the *P* receiver functions, the delay times of the negative phase vary between 7.4 to 8.0 s, in the *S* receiver function between 9.0 to 10.2 s.

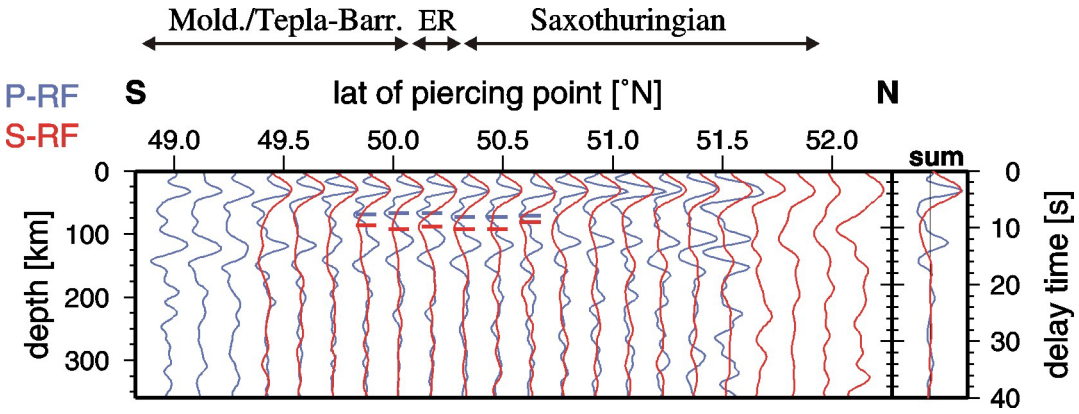

Figure 6.21: The same data profiles as in Figure 6.19, but corresponding traces of *P* and *S* receiver functions are super-imposed. The delay time of the Moho conversion signal is nearly identical in most traces. As in Figure 6.19, the maxima of the negative phases that arrive after the Moho *Ps* conversion are marked in the area of interest. In the *S* receiver functions, the negative phase arrives approximately 2 s later than in the *P* receiver functions.

It is not trivial to interpret these structures, because the frequency content of the two methods is different (*P* receiver functions have dominating wave periods around 1 s, while for *S* receiver functions wave periods around 5 s prevail) and hence also the resolution. At 80 km depth, a *P* wave with a period of 1 s and wave speed of 8 km/s has a wave length of λ=8 km. Assuming a vertical resolution of $\lambda/4$, a layer of at least 2 km thickness can be resolved by *P* receiver functions. An *S* wave with a period of 5 s and a wave speed of 4.5 km/s at 80 km depth has a wavelength of 23 km, which means that a layer must be at least 6 km thick to be detectable for *S* receiver functions. A thin layer of anomalous velocity might thus be detectable by *P* receiver functions and invisible in *S* receiver function data. A sharp gradient might be better visible in *P* receiver function data, while a broad gradient might be better to detect in *S* receiver function data.

Furthermore, due to the different geometry of the *Ps* and *Sp* rays, the incidence angles at the seismic interface and hence the conversion coefficients of the two ray types also differ, which influences the amplitude of converted energy.

Two scenarios are imaginable to explain the occurrence of the negative phase in the *P* and *S* receiver functions at slightly but significantly different delay times:

1) The negative phases in the *P* and *S* receiver functions represent two distinct discontinuities. A thin low velocity layer is detected by the *P* receiver functions in the lithospheric mantle at approximatel 65 km depth. As its thickness is between 2 and 6 km, it can not be detected by the *S* receiver function method. This low velocity layer could for example be caused by patches of partial melt. As the negative phase in the *P* receiver functions is observed in the area of CO_2 degassing and occurrence of earthquake swarms, a causal connection between the low velocity area at 65 km depth and these phenomena might be assumed. However, the negative gradient observed in *S* receiver function data at approximately 9 to 10 s is more or less coherent throughout the whole profile and might thus be interpreted as the lithosphere-asthenosphere transition. However, the thinning of the lithosphere proposed by *Babuška and Plomerová* (2001) would then not be obvious in the S

receiver function data, furthermore the diapiric mantle upwelling suggested by *Granet et al.* (1995) for the Bohemian Massif would show no imprint on the lithosphere-asthenosphere transition.

2) The negative phases in the *P* and *S* receiver functions represent in principle the same negative velocity gradient, but strongly influenced by the different frequency contents of the *P* and *S* waves and by the possible nature of the transition from high to low velocities with increasing depth. For example, if the gradient is steep at about 65 km depth and becomes increasingly less steep at 80 to 90 km depth, then *P* receiver functions would image also the steep part while *S* receiver functions would image also the flatter part of the gradient. However, as the negative phase in the *P* receiver functions is only observed in the broader surroundings of CO_2 degassing at surface and earthquake swarm occurrence, the proposed steep gradient zone would also occur only in this area. Again, this implies a thin region of strongly decreased seismic velocity at about 70 km depth which might be associated with the occurrence of partial melt in this depth range.